drones

MDPI

Article

Trajectory Optimization of a Subsonic Unpowered Gliding Vehicle Using Control Vector Parameterization

Ahmad Mahmood *, Fazal ur Rehman and Aamer Iqbal Bhatti

Department of Electrical Engineering, Capital University of Science & Technology, Islamabad 44000, Pakistan; frehman@cust.edu.pk (F.u.R.); aib@cust.edu.pk (A.I.B.)
* Correspondence: ahmad.mahmood.mughal@gmail.com

Abstract: In many aero gliding vehicles, achieving the maximum gliding range is a challenging task. A frequent example is the breakdown of an engine during flight or the use of unpowered stand-off weapons. When an unpowered stand-off weapon begins gliding at a given height, it eventually strikes the ground after some distance, and height is considered a stopping constraint in this general condition. To avoid the time-scaling approach for the free time optimal problem, the maximum stoppable time with a stopping constraint is addressed to attain the maximum glide range. This problem can be chosen as an optimal gliding range problem which can be solved by direct or indirect methods. In this paper, the inverted Y-tail joint stand-off weapon is selected as the subsonic unpowered gliding vehicle (SUGV). After being released from dispersion points, the SUGV has to face fluctuating gliding flight because of flight phase transition that causes gliding range reduction. To achieve a damped and steady gliding flight while maximizing the gliding range, we propose a non-uniform control vector parameterization (CVP) approach that uses the notion of exponential spacing for the time vector. When compared with the maximum step input and conventional uniform CVP approach, simulations of the proposed non-uniform CVP approach demonstrate that the SUGV exhibits superior damping and steady gliding flight, with a maximum gliding range of 121.278 km and a maximum horizontal range of 120.856 km.

Keywords: subsonic; unpowered gliding vehicle; gliding range maximization; control vector parametrization; stopping time; stopping constraint

Citation: Mahmood, A.; Rehman, F.u.; Bhatti, A.I. Trajectory Optimization of a Subsonic Unpowered Gliding Vehicle Using Control Vector Parameterization. *Drones* **2022**, *6*, 360. https://doi.org/10.3390/drones6110360

Academic Editor: Shiva Raj Pokhrel

Received: 11 October 2022
Accepted: 14 November 2022
Published: 17 November 2022

1. Introduction

Due to various controversies, the idea of aerial gliding vehicles (GVs) has evolved and matured over the time. Developments in the aviation industry led to the creation of both powered and unpowered GVs, where an unpowered GV relies on the dynamic interaction of the air with its wings and tail for gliding, and the velocity regime determines whether an unpowered GV is subsonic, transonic, supersonic, or hypersonic [1–4]. Nowadays, to convert a general purpose bomb (MK series) to a subsonic unpowered GV (SUGV), a wing adaptation kit or range extension kit is installed [5,6]. Figure 1 displays a further illustration of an SUGV known as the joint stand-off weapon (JSOW) [7].

Due to lack of propulsion, an SUGV is unable to follow the ballistic trajectories, resulting in limited gliding range and precision. Therefore, the aircraft has to get closer to solve these problems and neutralize the target, which decreases the aircraft's chances of evading enemy surveillance systems. To earn dispersion points, the pilot has to perform a series of aerobatic maneuvers and exercises to dodge enemy surface-to-air missiles and guns and to achieve the maximum glide range [8]. Factors such as incomplete adversary coordinate information, inaccurate dispersion points, variations in mass distribution, the center of gravity, aerodynamic characteristics, meteorological conditions, and the time delay between the practiced mission and the actual mission for the release of the SUGV reduce the gliding range. Consequently, accuracy and gliding range maximization are the most desirable objectives, and both objectives are linked to terminal guiding and gliding trajectory optimization.

As a problem of trajectory optimization, maximizing the SUGV's gliding range can be accomplished using either the direct or indirect method. The indirect method relies on Pontryagin's principle, which transforms an optimal problem into a two-point boundary value problem. On the other hand, the direct method transforms an optimal problem into a nonlinear programming problem by parameterizing the control or state variables and then calculating the problem using numerical methods. The main advantages of the direct method are that the necessary conditions are avoided and the parameterized variables are directly calibrated to optimize the performance index.

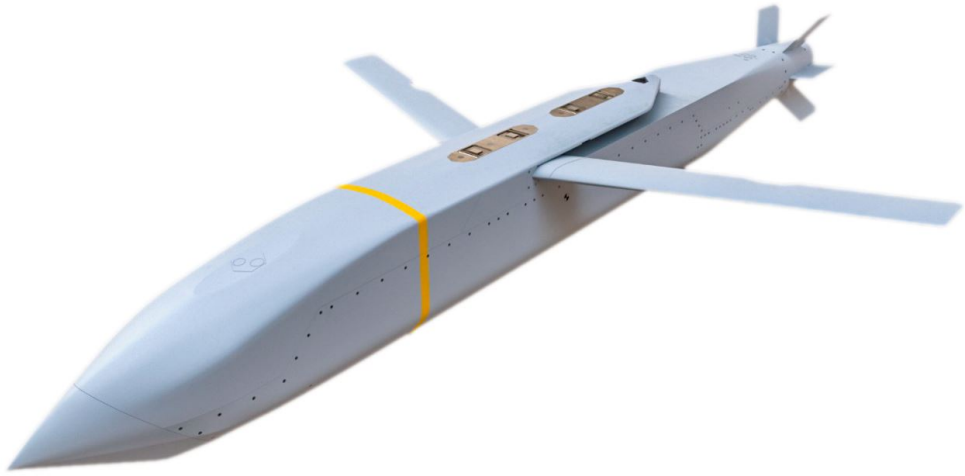

Figure 1. Joint stand-off weapon (JSOW).

Sheu et al. [9,10] attempted to determine the maximum horizontal range for unpowered GVs in a three-dimensional space. The authors of these publications intended to give a comparison of the singular perturbation method and the second-order gradient approach linked with Pontryagin's maximum principle. The second technique involves using closed-loop control to modify high-speed conditions such as the altitude and flight path angle to maximize productivity. Chern et al. [11] studied gliding flight for its maximum range while taking the horizontal distance and endurance into account and arrived at a solution based on Pontryagin's maximimum principle. To maximize the glide distance of an unpowered guided projectile, the effects of fin deployment and autopilot delay were examined in [12], and the Hamiltonian boundary value problem was solved using a variational calculus technique. To govern the flight, Yu et al. [13] suggested range optimization-guiding legislation that suppressed phugoid oscillations with angle-of-attack feedback. A combined guidance algorithm for gun-launched, rocket-assisted guided projectiles was developed to maximize the flight range and endurance in [14]. Zhang et al. [15] released an investigation of the maximum gliding range along with a guidance scheme based on the flight path angle for SUGVs. They also established an inverse relationship between the lift/drag ratio and dynamic pressure to calculate the optimum lift/drag ratio responsible for the maximum glide range. Using the Radau pseudospectral approach, Yuan et al. [16] explored the maximum glide range of a glide-guided bomb. In this work, the principle of covector mapping is applied to compute the optimal gliding trajectory. To optimize the gliding trajectory of a gun-launched unpowered gliding weapon, the hp-adaptive pseudospectral technique, a trajectory optimization approach, was studied in [17]. After disconnecting the booster, Qiu et al. [18] addressed the problem of the GV's maximum downrange. By considering the Legendre–Gauss–Radau collocation points, the nonlinear optimization issue was converted into a nonlinear programming problem. Then, to optimize the downrange, a pseudospectral technique with adaptive mesh refinement was used. Gao et al. [19] created virtual control derivatives for gliding vehicles in re-entry to calculate the best

control solution and acquire the optimal range solution using the hp-adaptive pseudospectral approach. Xiao et al. [20] introduced an enhanced version of the adaptive Gaussian pseudospectral approach to tackle the nonlinear constraint management issue and increase the glide vehicle's downrange, and they showed the feasibility of this novel approach by comparing it to the standard adaptive Gaussian pseudospectral method. An et al. [21] sought to tackle the problem of maximizing the gliding trajectory of a boost-glide vehicle. They separated the total technique into two stages. In the first stage, a pitch angle-based climb guidance law and descent guidance legislation based on the angle of attack are formulated, and in the second stage, a Legendre–Gauss–Radau orthogonal collocation approach is used to discretize the state and control variables, after which the optimization problem is converted into a nonlinear programming problem, and then sequential quadratic programming is used to optimize the gliding range.

Shapira et al. [22] introduced the singular perturbation theory to optimize the range by taking timescale separation and dynamic effects into consideration. They also used a dichotomic basis method to build an indirect solution for optimum control over two timescales. Considering an engine failure scenario, Feng et al. [23] paid attention to increasing the gliding range as well as endurance through the FALCON.m tool. In the gliding range, wind or ground influences may reduce the gliding range [24]. Ben Asher et al. [25] employed the pseudo-spectral technique based on the GPOPS tool to improve the gliding profile while taking into consideration the impact of the wind to cater to the engine cutoff issue. In the presence of along-track wind, Franco et al. [26] used the optimal control singular arc theory to obtain the maximum range. Moreover, the implications of the average wind and wind shear on the optimal outcomes were investigated. However, they did not take into account crosswinds and the unpowered descent trajectory, which are treated as state inequality constraints. The Chebyshev pseudospectral technique was applied to calculate the maximum glide range of an aircraft in the presence of wind in [27]. Segal et al. [28] released a glide range maximization algorithm for engine-out aircraft that ensured a constant heading and velocity during descent flight. They also developed a relationship for the maximum glide speed that depends on the speed of the aircraft in the presence of still air and windy environments.

Creating wings, tails, and fins with precise geometry also helps to enhance the standoff distance. Using empirical and non-empirical approaches, the unpowered aerodynamic model is optimized to yield the maximum glide range [29,30]. Elsherbiny et al. [31] published a solution for optimal aerodynamic lifting surfaces to increase the gliding range using hybrid optimization algorithms integrated with missile DATCOM. A particle swarm optimization approach was employed in conjunction with missile DATCOM to optimize the shape, fin size, and position of the control surfaces for a given projectile's gliding range [32]. Under the guise of machine learning and neural networks, artificial intelligence has demonstrated promising results in optimal theory [33]. Reinforcement learning, a subtype of machine learning, has the capacity to learn through trial and error as a consequence of rewards from the system dynamics. As the dynamics of the system change, the reward is optimized. To obtain the optimal gliding performance of a subsonic, fixed-wing, unmanned aerial vehicle, Din et al. [34–36] applied reinforcement learning algorithms such as DDPG, TRPO, PPO, and MRL.

The gliding path of an SUGV can be considered an optimal control problem with inequality constraints and highly nonlinear dynamics. A direct method, specifically control vector parameterization (CVP) [37], can be used to deal with the optimal gliding trajectory and optimal path planning problems [38,39]. Because of its high performance, simplicity, and flexibility, CVP is very appealing. Therefore, several fields have recently successfully incorporated the CVP approach [40–43]. The time vector's division, which may be uniform or non-uniform, is a key factor in the CVP approach [44–48]. To extend the downrange of a hypersonic unpowered GV, Liu et al. [49] developed a constraint handling method with a smoothing methodology based on a uniformly distributed CVP approach. Teo et al. [50] employed a uniformly distributed time vector-based CVP approach to solve the challenge

of optimizing the range of a subsonic flying object and succeeded by combining the CVP approach with Pontryagin's principle. Liu et al. [51] proposed employing an adaptive control arc length-based trajectory optimization methodology that combines the CVP method with a Gauss time grid distribution and an adaptive time grid refinement procedure to increase the downrange performance of a hypersonic GV after the re-entry phase. To increase the hypersonic unpowered GV range, Hui et al. [52] combined the conventional CVP approach with an improved sparrow search algorithm and a time-scaling approach. They also used the golden sine update strategy and tent chaotic sequence mapping to obtain the initial guess efficiency and optimality.

When the SUGV begins gliding from the dispersion points, it transitions from wing-level flight to gliding flight. This flight transition causes fluctuations in the gliding flight, and these fluctuations reduce the gliding range. Damped and steady gliding flight is required to reduce this effect and maximize the gliding range. In most of the aforementioned work, the gliding range was enhanced by maximizing the lift/drag ratio, finding the optimal geometric configuration, and employing guidance laws to counteract the windy effects during gliding flight. The effects of fluctuations caused by flight transition were not taken into account to maximize the gliding range. To overcome this problem, we propose a non-uniform CVP approach based on the notion of exponential spacing for the time vector. The authors of [53] used a uniform CVP to maximize the gliding range. They solved the optimization problem using a time-scaling approach that introduced a new variable which should be treated either as an additional control input or as an optimal variable that increases the complexity of the problem. In this work, instead of a time-scaling approach, we define a predetermined maximum stoppable time and set the height as the stopping constraint.

The overall contributions of this work are as follows:

- Fluctuations caused by flight transition are minimized using a non-uniform CVP approach, and damped and steady gliding flight is achieved to maximize the gliding range;
- By defining the maximum stoppable time with the height as the stopping constraint, the complexity of the optimization problem is decreased;
- The results of the non-uniform CVP approach are compared with those of the uniform CVP approach and those of the maximum step input.

The following is a description of the remaining structure of this paper. In Section 2, a general overview of SUGV modeling is covered. The problem of the maximum gliding range at the maximum stoppable time is detailed in Section 3. Section 4 describes the proposed CVP approach, which is based on the time vector's exponential spacing. The simulations and performance findings between the uniform CVP and the suggested CVP are shown in Section 5. The conclusions of the work are briefly described in Section 6.

2. SUGV Modeling Overview

The SUGV mathematical model was selected based on the following assumptions:

- A constant mass and gravity field;
- Rigid body dynamics;
- Non-rotating and flat earth.

A longitudinal model was adopted to demonstrate the reliability of SUGVs and a demonstration of the aerodynamic forces of lift L, drag D, and weight W on an SUGV, with the pitching moment M along the y-axis and airspeed along the x-axis, are expressed in Figure 2. Elevators are positioned on the inverted Y-tail and serve as control inputs.

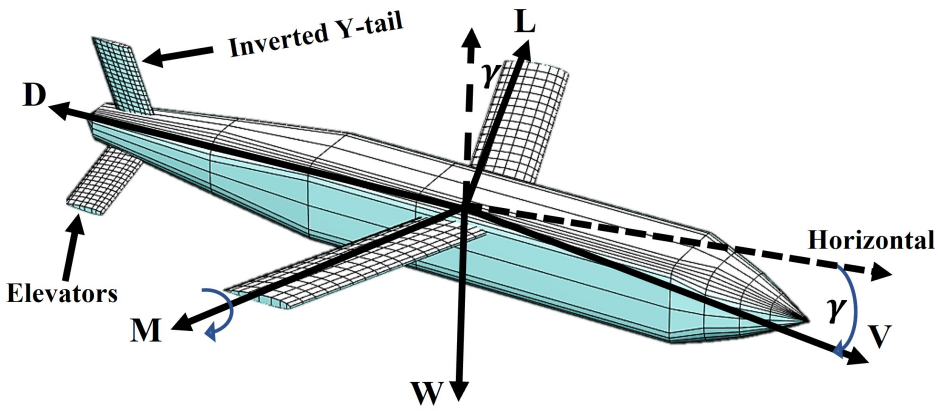

Figure 2. Representation of forces and moment on SUGV.

2.1. Longitudinal Dynamics

The SUGV longitudinal dynamic model is illustrated as follows:

$$m\dot{V} = -D - W\sin(\theta - \alpha) \tag{1}$$

$$m\dot{\alpha} = -\frac{L}{V} + \frac{W}{V}\cos(\theta - \alpha) + mQ \tag{2}$$

$$\dot{Q} = \frac{M}{I_y} \tag{3}$$

$$\dot{\theta} = Q \tag{4}$$

where V, α, Q, θ, and I_y stand for the airspeed, angle of attack, pitch rate, pitch angle, and pitching moment of inertia, respectively, and γ shows the flight path angle. D expresses the drag force, L presents the lift force, W shows the weight during the flight, and M yields the pitching moment. The path of an unpowered gliding flight is represented by the following navigation equations:

$$\dot{R} = V\cos(\theta - \alpha) \tag{5}$$

$$\dot{h} = V\sin(\theta - \alpha) \tag{6}$$

where R and h express the distance along the x-axis and the distance along the z-axis, respectively.

2.2. Aerodynamic Forces and Moments

The expressions for the longitudinal aerodynamic forces and the pitching moment are as follows:

$$D = 0.5\rho V^2 S C_D \tag{7}$$

$$L = 0.5\rho V^2 S C_L \tag{8}$$

$$W = mg \tag{9}$$

$$M = 0.5\rho V^2 S \bar{C} C_M \tag{10}$$

where S is the wing reference area, $\bar{C}$ is the wing mean aerodynamic chord, and ρ signifies the air's density, which is represented by

$$\rho = 1.222 - 1.15e^{-4}h + 3.18e^{-9}h^2 \tag{11}$$

The drag, lift, and pitching moment coefficients are determined using the flying factors and geometric configuration of the SUGV. Therefore, these coefficients are defined as follows:

$$C_L = C_{L_\alpha}(Mcn, \alpha, h)\alpha + C_{L_Q}(Mcn, \alpha, h)Q\frac{\bar{C}}{2V} + C_{L_{\delta_e}}(Mcn, \alpha, h)\delta_e \tag{12}$$

$$C_D = \frac{C_L^2}{2\pi eAR} + C_{D_{\delta_e}}(Mcn, \alpha, h)\delta_e \tag{13}$$

$$C_M = C_{M_\alpha}(Mcn, \alpha, h)\alpha + C_{M_Q}(Mcn, \alpha, h)Q\frac{\bar{C}}{2V} + C_{M_{\delta_e}}(Mcn, \alpha, h)\delta_e \tag{14}$$

where $C_{L_{\delta_e}}$, $C_{D_{\delta_e}}$ and $C_{M_{\delta_e}}$ stand for the partial derivative of lift, drag, and pitching moment with respect to the elevator deflection δ_e. C_{L_α}, C_{D_α}, and C_{M_α} point out the partial derivative of lift, drag, and pitching moment with respect to α, respectively. C_{L_Q}, C_{D_Q}, and C_{M_Q} are the partial derivative of lift, drag, and pitching moment with respect to Q, respectively. Moreover, e is the Oswald efficiency number, and AR is the aspect ratio of the SUGV.

3. Problem Description

Consider the nonlinear system

$$\dot{X} = f(X, u) \quad t_0 \leq t_s \leq t_m \tag{15}$$

$$X^o = X(t_0) \tag{16}$$

where $X = (V, \alpha, Q, \theta, R, h)^T \in \Re^6$, X^o is the initial state, t_0 is the starting time, and t_m is the maximum stoppable time. For a nonlinear system, the stopping manifold is defined as follows [53,54]:

$$S_m = \{\Delta(X) = 0, X \in \Re^6\} \tag{17}$$

where Δ is a continuously differentiable function. When the system reaches the manifold S_m, it comes to a halt, and the time it took to get there is referred to as the stopping time t_s, which relies on the stopping constraint. A graphical representation of S_m and t_s is shown in Figure 3.

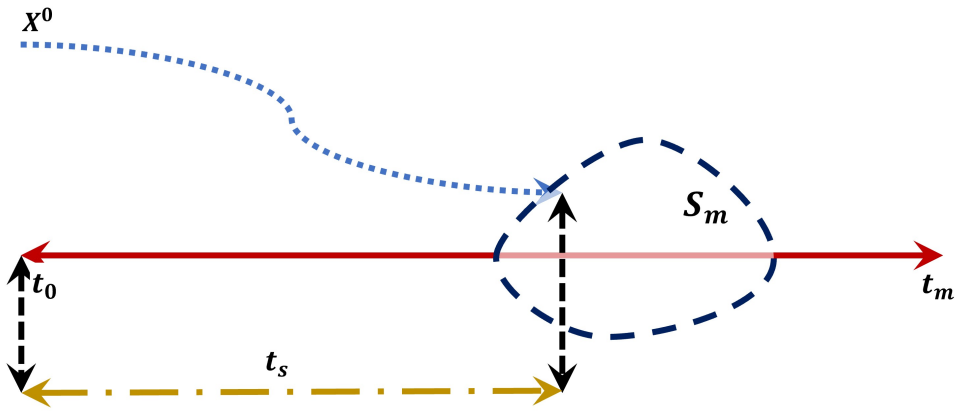

Figure 3. Stopping manifold.

Here, t_s is an implicit function of the control input u, since any change in u impacts the state response, resulting in a change in t_s. The stopping time is determined as follows:

$$\tau_u = \{t_0 < t \leq t_m,\ X(t|u) \in S_m\} \tag{18}$$

$$t_s = \inf_t\{\tau_u\} \tag{19}$$

Any $t_s \in \tau_u$ is expressed as an admissible stopping time, and if $t_s \leq t_m$, then the stopping constraint is computed as follows:

$$\Delta(X(t_s))|_{\tau_u} = 0 \tag{20}$$

A performance index for t_s is established as follows:

$$J = \int_{t_0}^{t_s} X(t)\, dt \tag{21}$$

Constraints on the states and control input are expressed as

$$x^L \leq X(t) \leq x^U \quad \forall\, t \in (0, t_s \leq t_m) \tag{22}$$

$$u^L \leq u(t) \leq u^U \quad \forall\, t \in (0, t_s \leq t_m) \tag{23}$$

where x^L, u^L and x^U, u^U are the lower and upper constraints on the states and control input, respectively.

3.1. Performance Index

The fundamental goal of unpowered gliding flight is to maximize the SUGV's gliding range, and for this purpose, a Lagrange performance index is illustrated:

$$J = max \int_{t_0}^{t_s} V\, dt \tag{24}$$

A subsidiary state is suggested to avoid integral complexity in the performance index:

$$\dot{\aleph} = V \quad \forall\, t \in (0, t_s \leq t_m) \tag{25}$$

After augmenting Equation (24) with the longitudinal dynamics of an SUGV, the performance index can be expressed in Mayer form as follows:

$$J_{\aleph} = max\ \aleph(t_s) \tag{26}$$

3.2. Constraints

Let α be significant during gliding flight for an SUGV. If it is small, then it causes a free fall condition, and if it is large, then it creates a stall condition. Therefore, α needs to be limited. Furthermore, Q aids in the reduction in fluctuations produced by flight transition and offers stability during gliding flight. Therefore, a constraint on Q is required to decrease the influence of fluctuations. To achieve damped gliding flight, both constraints are implemented, and these constraints are

$$\begin{cases} \alpha^L \leq \alpha(t) \leq \alpha^U \\ Q^L \leq Q(t) \leq Q^U \end{cases} \quad \forall\, t \in (0, t_s \leq t_m) \tag{27}$$

where α^L, Q^L, α^U, and Q^U are the lower and upper constraints on α and Q, respectively. The load factor (*LF*) ensures the wing-level flight by imposing the constraint during gliding flight so that steady gliding flight can be obtained. Therefore, a constraint on *LF* is employed to assure a steady gliding flight and is defined as

$$LF = \frac{\sqrt{L(t)^2 + D(t)^2}}{W} \leq LF_{max} \quad \forall\, t \in (0, t_s \leq t_m) \tag{28}$$

where LF_{max} is the maximum value of LF. A constraint on elevator deflection is applied to elude the stall condition during gliding flight as follows:

$$\delta_e^L \leq \delta_e(t) \leq \delta_e^U \quad \forall\, t \in (0, t_s \leq t_m) \tag{29}$$

where δ_e^L and δ_e^U are the lower and upper bounds on the elevator deflection, respectively. The height from the dispersion point steadily decreases to zero until the SUGV strikes the earth. As a result, in this study, the height is regarded a stopping constraint:

$$h(t_s) = 0 \tag{30}$$

Problem: Maximize the SUGV's gliding range by incorporating the performance index in Equation (26), the dynamic system in Equations (1)–(6) with Equation (25), the damping constraints in Equation (27), the LF constraint in Equation (28), the stopping constraint in Equation (30) and the elevator deflection constraint in Equation (29).

4. Control Vector Parameterization

In this section, the concept of control vector parameterization (CVP) with uniform and non-uniform subintervals is discussed. CVP is a very straightforward notion because the time vector of an optimization problem is broken into a predetermined number of subintervals, the beginning and end of which are referred to as nodes in the CVP process. Then, the control variables are selected at certain nodes, known as nodal control variables. The control profile is then built using a spline approach, such as piecewise linear polynomials or piecewise constant functions. After this, the dynamic model is integrated, referred to as the initial value problem (IVP). After computing the IVP, the nodal control variables are subjected to a nonlinear programming approach in order to optimize the problem. The transformation of the infinite-dimension optimization problem into a finite-dimension optimization problem by taking into account a predefined number of nodal control variables is a key feature of CVP. A general description of the CVP procedure is given below:

(i) Specify the desired $N > 1$ number of nodes and split the supplied time vector t_m into $N - 1$ subintervals:

$$t_i = t_0 < t_1 < t_2 < \cdots < t_{N-1} = t_m \tag{31}$$

The nodal time $t_i, i = 0, 1, 2, \ldots N - 1$ may be uniform or non-uniform.

(ii) At each node, make an initial guess for the control variable. The following control vvector (CV) u(t) is expressed as

$$u(t) = [\overline{u}_0, \overline{u}_1, \overline{u}_2, \ldots \overline{u}_{N-1}] \tag{32}$$

where $\overline{u}_i, i = 0, 1, 2, \ldots N - 1$ is a nodal control variable.

(iii) Use an interpolation polynomial to approximate the CV profile.

(iv) Solve the IVP by considering the approximated CV profile.

(v) Compute the performance index as well as the constraints. If the performance index and constraints are satisfied, then the output will be the optimal solution; otherwise, proceed to step (iii) after optimizing the nodal control variables with any suitable optimizer.

Figure 4 depicts a flowchart describing the CVP implementation process.

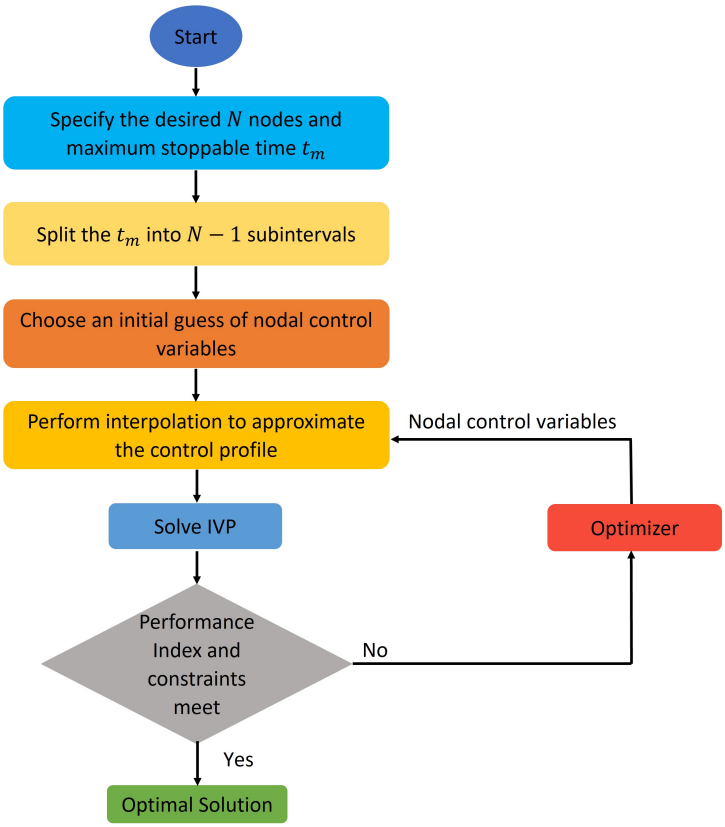

Figure 4. CVP procedure.

4.1. Uniform CVP

We will provide a brief overview of the uniform subinterval method for CVP in this subsection. This method divides the time vector $t \in (t_o, t_m)$ into $N-1$ subintervals for the maximum stoppable time t_m. For a uniform subinterval, the subinterval size d_e is assessed as follows:

$$d_e = \frac{t_m - t_0}{N-1} \tag{33}$$

Consequently, the nodal times t_i for a uniform time vector are determined as follows:

$$t_i = t_o + id_e \quad i = 0, 1, 2, \ldots, N-1 \tag{34}$$

In Figure 5, the uniform CV approach with nodal times $t_o, t_1, \ldots, t_m$ and nodal control variables $\overline{u}_0, \overline{u}_1, \overline{u}_2, \ldots \overline{u}_{N-1}$ at uniform subintervals are graphically depicted.

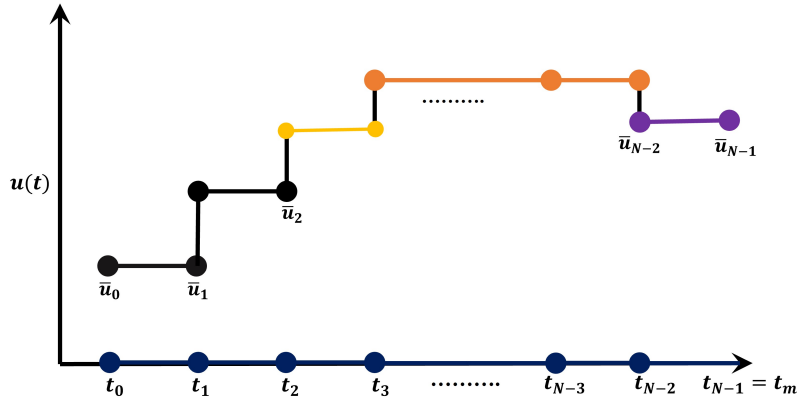

Figure 5. Uniform CVP.

4.2. Non-Uniform CVP

After the acquisition of the dispersion points, the SUGV enters the disequilibrium phase, and fluctuations occur during gliding as a result of this phase change. Fast damping may be performed quickly to lessen fluctuations by establishing constraints on α and Q. To achieve a steady glide path, the load factor is also crucial. Consequently, a non-uniform CVP strategy is required to more effectively address these problems. On the foundation of the idea of exponential spacing, a new formulation for non-uniform subintervals is presented. According to this formulation, the time vector $t \in (t_o, t_m)$ is broken into $N-1$ subintervals, and low spacing happens at the beginning of the time vector, whereas large spacing occurs toward the end. Assume that μ_o and $log_{10}(\chi)$ represent the lower and upper bounds of an exponential curve 10^a in a logarithmic scale. For computing the logarithmic vector, the interval size Y is calculated using these bounds as follows:

$$\mathrm{Y} = \frac{log_{10}(\chi) - \mu_o}{N-1} \tag{35}$$

Notably, μ_o will always be set to zero, and the logarithmic vector ℓ is computed as follows:

$$\ell = \mu_o + i\mathrm{Y} \quad i = 0, 1, 2, ..., N-1 \tag{36}$$

Using ℓ, the following relation is given to obtain an exponential vector T_{exp}:

$$T_{exp} = 10^{\ell} - 1 \tag{37}$$

Hence, the relation shown below is used to map the maximum stoppable time onto an exponential vector:

$$T = \frac{t_m - t_0}{T_{exp}^{max}} T_{exp} \tag{38}$$

where χ is exponential spacing factor with an inverse relation with the exponential spacing of the time vector T and is the upper bound of the exponential curve 10^a. Figure 6 depicts a graphical representation of the non-uniform CVP approach based on exponential spacing of the nodal times $T_o, T_1, \ldots, T_{N-1} = t_m$ and nodal control variables $\overline{u}_0, \overline{u}_1, \overline{u}_2, \ldots \overline{u}_{N-1}$.

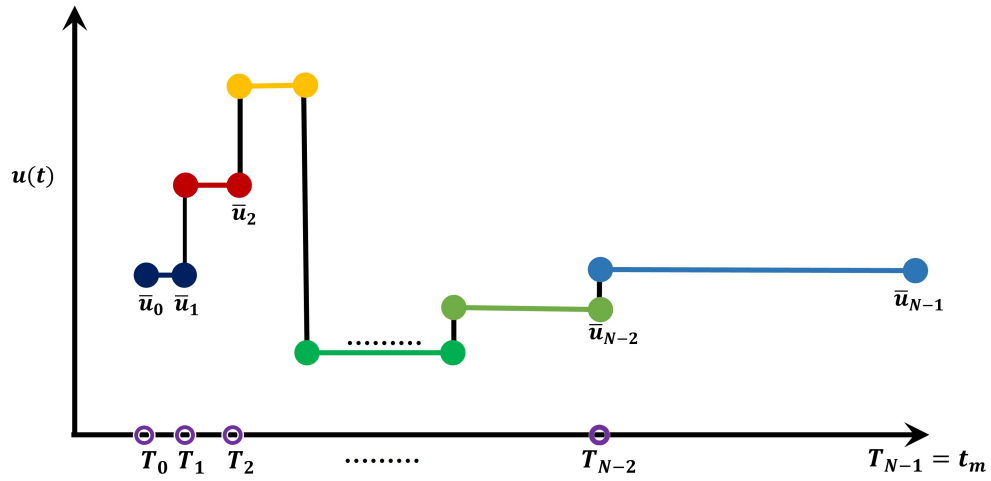

Figure 6. Non-uniform CVP.

A derivation procedure of exponential spacing-based non-uniform CVP is shown in the Figure 7 below.

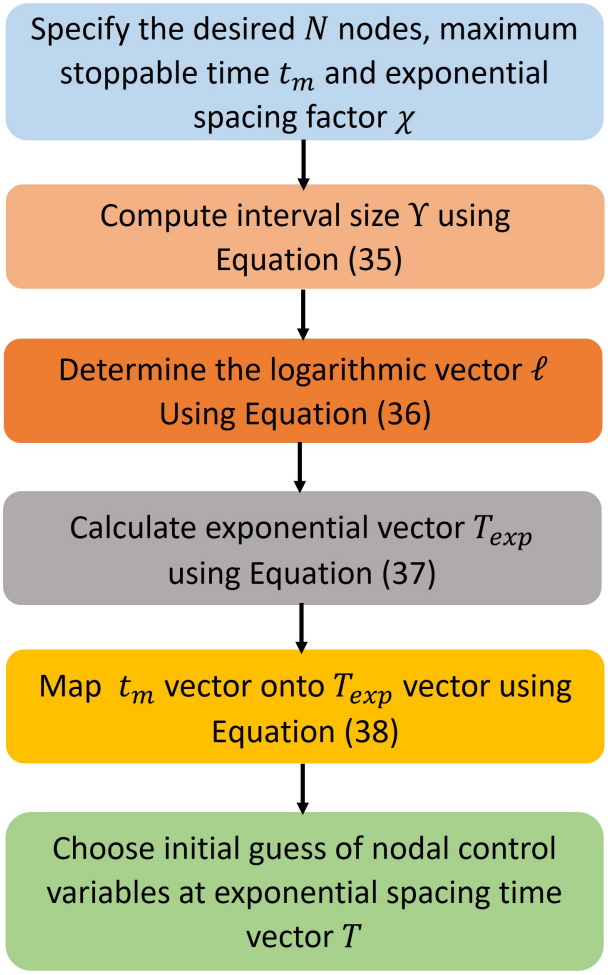

Figure 7. Derivation procedure of non-uniform CVP.

5. Simulation Results

The feasibility and effectiveness of the exponential based non-uniform CVP approach for an SUGV's gliding range is compared with the maximum elevator step δ_e and classical uniform CVP approach in this section. The maximum gliding range was calculated using *MATLAB* and *DS Simulia Isight*. For performance progression, we set t_m to 850 s and N to 10, 15, and 20. A time vector with a specified N had its χ able to be adjusted as desired. Simulations of the SUGV range maximization were performed using the dispersion points [6] given in Table 1.

Table 1. SUGV Dispersion points.

States	Dispersion Points
V	0.72 Ma
α	0 deg
Q	0 deg s^{-1}
θ	0 deg
R	0 km
h	10 km

To achieve the maximum glide range using the CVP approach, we borrowed the bounds on α and δ_e from [6,35], respectively, and then used the hint in [55] to establish the constraint on *LF*. We arrived at a constraint that fit our problem-solving criterion by examining the impact of several restrictions on Q, and all constraints are listed in Table 2.

Table 2. SUGV constraints.

Angle of Attack (deg)	Pitch Rate (deg s^{-1})	Load Factor	Elevator Deflection (deg)
$0 \leq \alpha \leq 2.65$	$-1 \leq Q \leq 1$	LF ≤ 1.007	$0 \leq \delta_e \leq 6$

5.1. Case 1: N = 10

Figure 8 depicts the simulation results for 10 nodes, comparing the proposed CVP approach with the maximum step input of 6 deg and the conventional CVP approach.

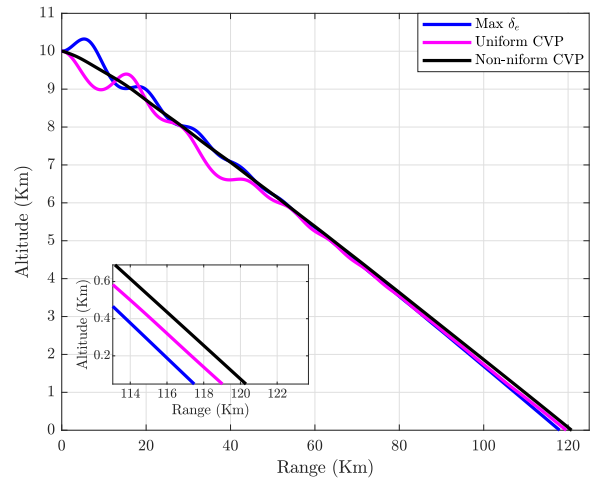

(**a**)

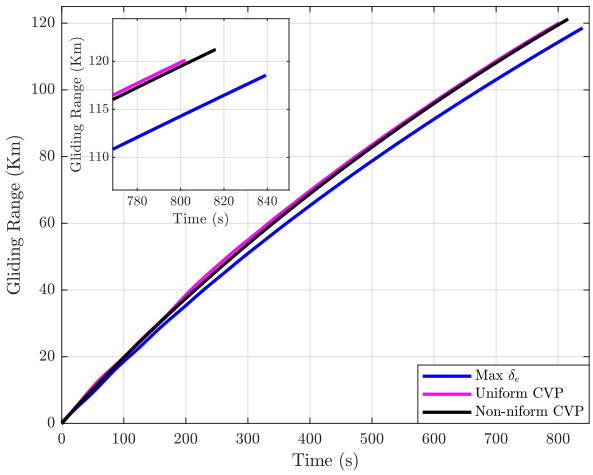

(**b**)

Figure 8. *Cont.*

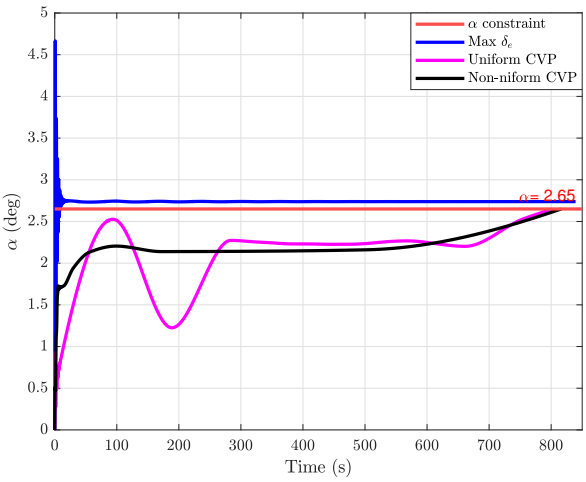

(c)

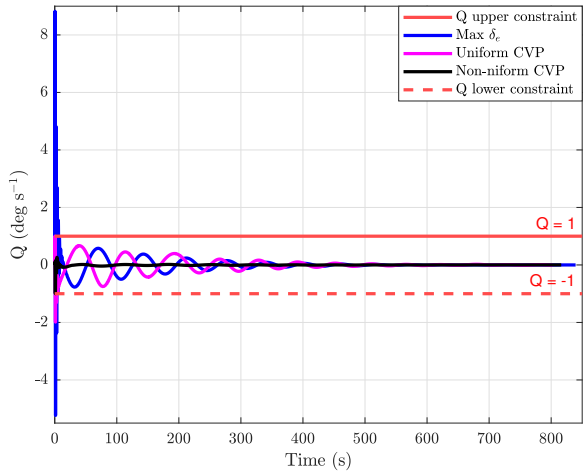

(d)

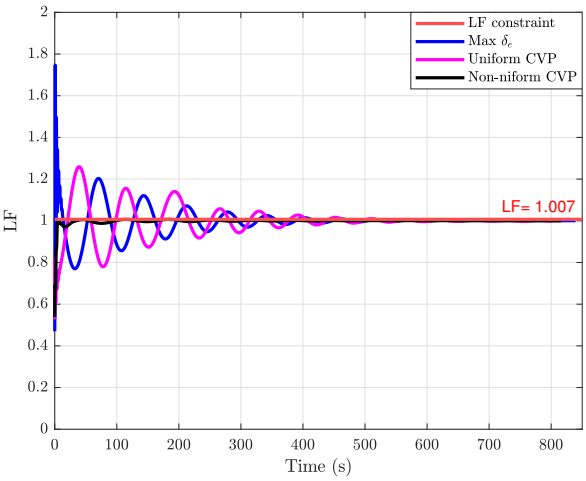

(e)

Figure 8. *Cont.*

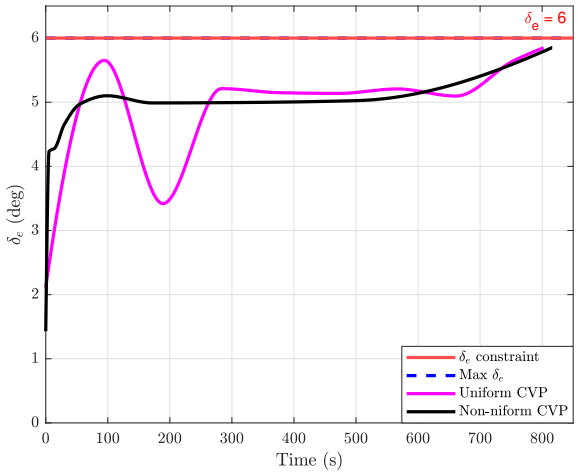

(**f**)

Figure 8. Non-uniform CVP for N = 10: (**a**) gliding trajectory, (**b**) gliding range, (**c**) angle of attack constraint, (**d**) pitch rate constraint, (**e**) load factor constraint, and (**f**) elevator constraint.

In the uniform CVP approach, the optimizer tried to obtain faster damping to generate steady gliding flight compared with the maximum step input. Figure 8a shows that when the SUGV dropped from the carrier platform, the optimizer produced a low angle of attack, which induced free fall, and then the optimizer tried to stabilize the gliding flight. As demonstrated in Figure 8a, the non-uniform CVP approach provided excellent results for fast damping and steady gliding flight, reducing the impacts of fluctuations and increasing the gliding range by 121.25 km. The variation in constraint profiles is shown in Figure 8c–e. Uniform CVP met the α requirement, with variations that stabilized after 280 s, but non-uniform CVP had a smooth α profile. The findings for the Q constraint demonstrate that the non-uniform CVP approach beat the other reference approaches when it came to performance. The uniform CVP approach sought to keep the Q profile between the limits but was unsuccessful. Figure 8e for the uniform CVP approach and maximum step input illustrates a violation and considerable variability in the load factor constraint profile. The non-uniform CVP approach, on the other hand, provided a less-varying load factor constraint profile that assured steady gliding flight. Comparatively, the constraint profiles illustrate the maximum range progression and efficacy for the SUGV in addition to the suggested CVP approach for steady gliding flight. The non-uniform CVP approach generated a control profile with less variability and less amplitude than the uniform CVP approach, as shown in Figure 8f, ensuring the optimal gliding range and achieving steady gliding flight with less pressure on the elevator actuators.

5.2. Case 2: N = 15

Figure 9 illustrates the simulation outcomes with 15 nodes for the maximum step input of 6 deg, the conventional uniform CVP approach, and the proposed non-uniform CVP approach. By increasing the number of nodes, the control profile for the uniform CVP method became more variable, hence affecting the glide path. Uniform CVP for 15 nodes resulted in less free falling behavior than the uniform CVP for 10 nodes. In the uniform CVP strategy, the optimizer attempted to raise the alpha value closer to the ground to maximize the gliding range relative to the maximum elevator input. The uniform CVP technique did not provide promising results in terms of damped and steady gliding flight, but Figure 9a,b illustrates that the suggested non-uniform CVP approach produced fast damping and steady gliding flight.

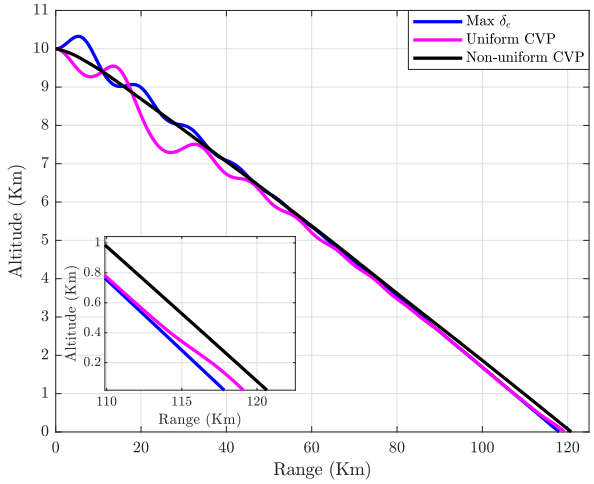

(**a**)

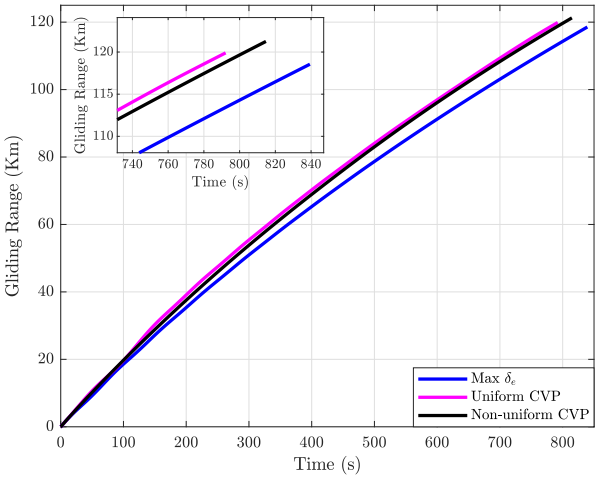

(**b**)

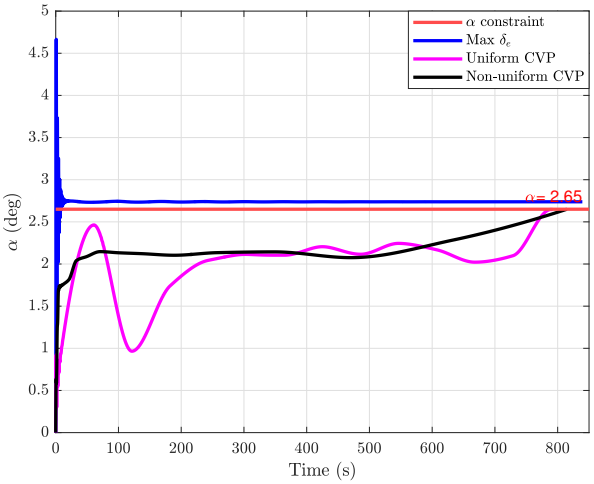

(**c**)

Figure 9. *Cont*.

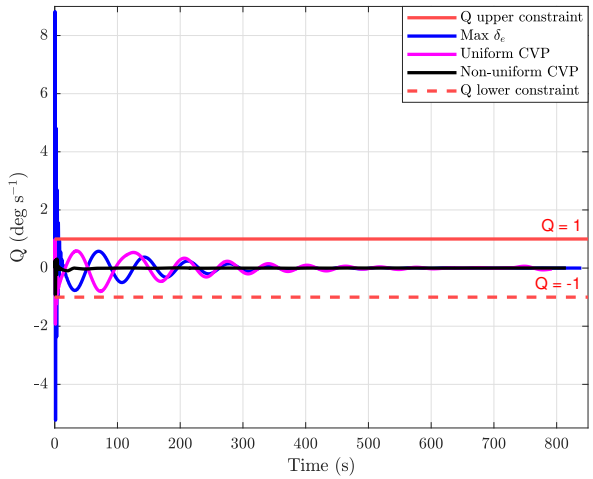

(**d**)

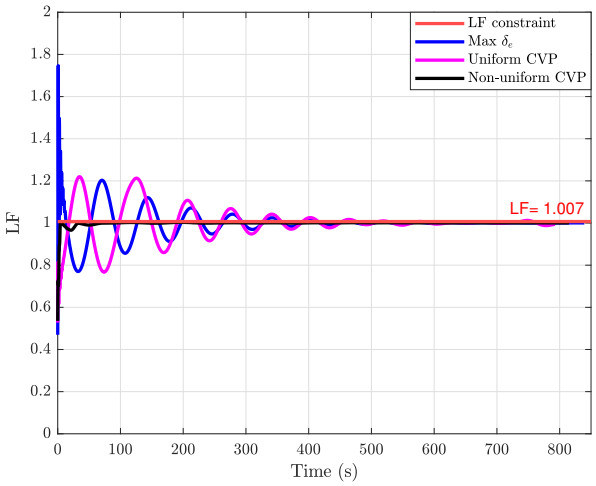

(**e**)

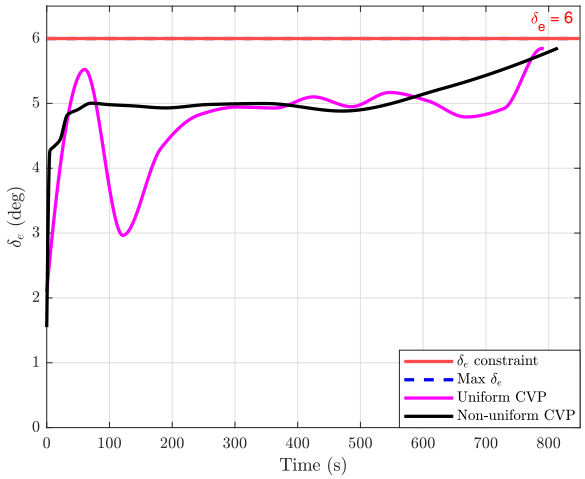

(**f**)

Figure 9. Non-uniform CVP for N = 15: (**a**) gliding trajectory, (**b**) gliding range, (**c**) angle of attack constraint, (**d**) pitch rate constraint, (**e**) load factor constraint, and (**f**) elevator constraint.

The suggested non-uniform CVP approach obtained a gliding range of 121.26 km and a horizontal range of 120.84 km, which are both encouraging results in damped and steady gliding flight when compared with the approaches discussed. Figure 9c–e demonstrates the constraint profile. Due to the increase in the number of nodes for the uniform CVP approach, the α constraint exhibited significant variance, while the suggested non-uniform CVP approach resulted in a negligible variance in the α constraint after commencement of gliding flight. Despite the uniform CVP approach's attempts to limit oscillations in the Q constraint profile, the lower bound was exceeded. The suggested non-uniform CVP method met the Q restrictions, and node increases caused saturation in the lower spacing of the CV, with this impact seen in the Q profile. The LF profile demonstrates that the non-uniform CVP approach yielded a profile with little variation while meeting the requirement that ensured steady gliding flight. The constraint on the control input is expressed in Figure 9f. Despite the increase in the number of nodes, the control profile demonstrates that the suggested non-uniform CVP provided less stress on the elevator actuators and a smooth profile with little variance.

5.3. Case 3: N = 20

The optimal outcomes based on 20 nodes for the proposed non-uniform CVP, maximum step input, and uniform CVP are shown in Figure 10.

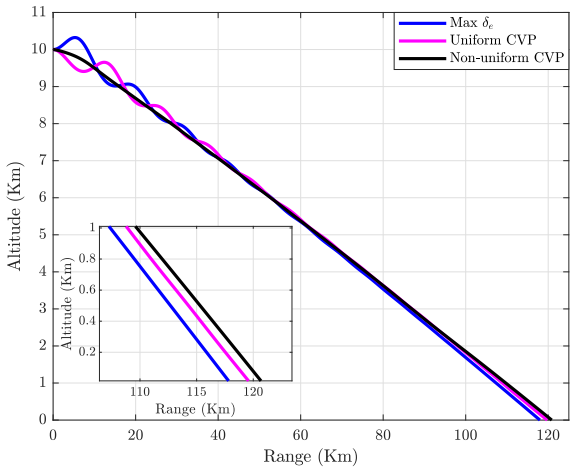

(**a**)

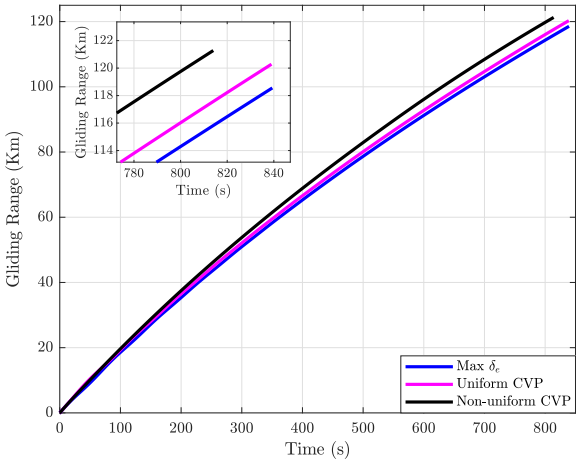

(**b**)

Figure 10. *Cont.*

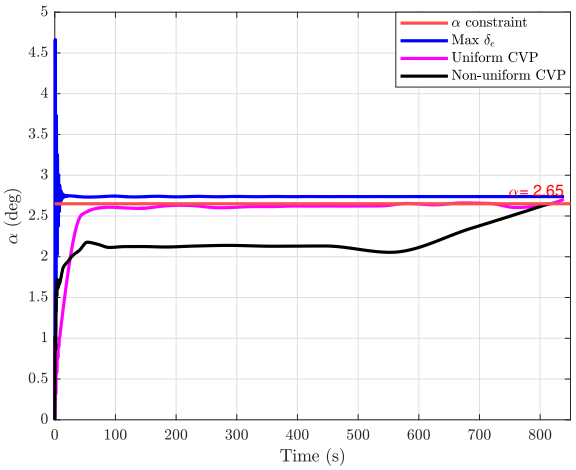

(**c**)

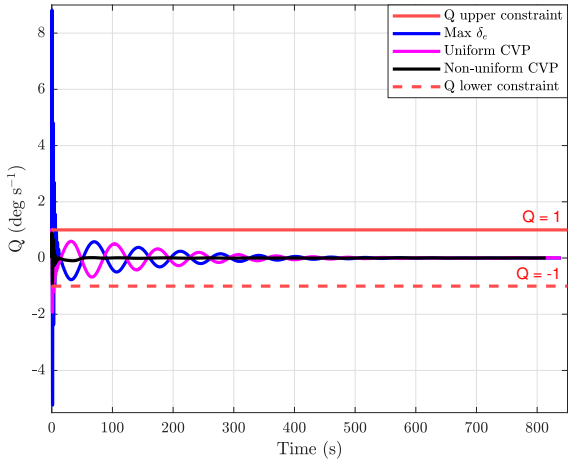

(**d**)

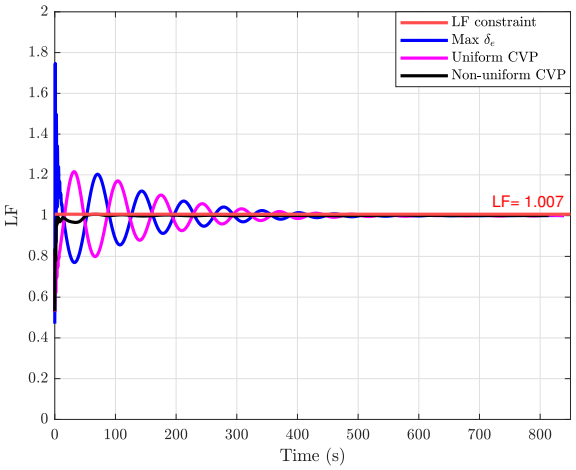

(**e**)

Figure 10. *Cont.*

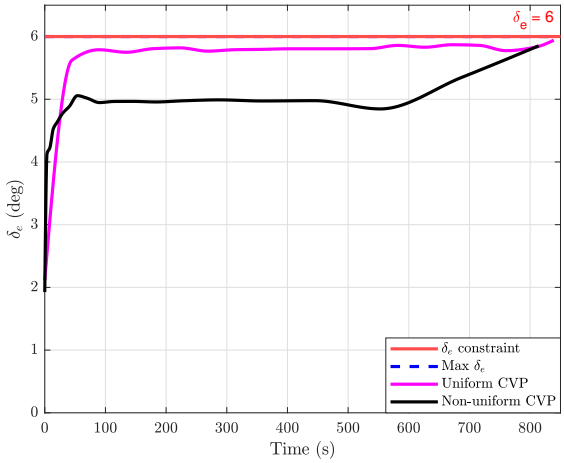

(**f**)

Figure 10. Non-uniform CVP for N = 20: (**a**) gliding trajectory, (**b**) gliding range, (**c**) angle of attack constraint, (**d**) pitch rate constraint, (**e**) load factor constraint, and (**f**) elevator constraint.

Figure 10 demonstrates that the optimizer tried to calculate damped and steady gliding flight using a uniform CVP approach in contrast to the maximum step input results, while the uniform CVP technique resulted in fewer free fall situations than the prior cases. The proposed non-uniform CVP method effectively generated an optimal gliding trajectory to address sluggish damping and unsteady gliding flight issues, and it optimized the gliding range to 121.28 km and the horizontal distance to 120.856 km. The uniform CVP approach, unlike the maximum step input, decreased the magnitude of the changes in Q and α but did not result in damped and steady gliding flight. Figure 10c–e illustrates the significance of the suggested non-uniform CVP method via the modification of restrictions. The non-uniform CVP method provided the constraint results with a damped profile and satisfied the constraint values, but the suggested CVP revealed the increase in the number of nodes as saturation in the load factor. Figure 10f portrays the optimal control input profile. It can be observed that the uniform CVP method caused a minimal change in the input profile with low actuator pressure. To optimize the gliding range, it was found that the optimizer for the proposed CVP method mimicked the best control profile, with a tiny variance owing to the node increase at the outset.

The maximum values of the constraint profiles for the chosen techniques are shown in Table 3 for numerical observation. It can be seen that the constraint profiles of the non-uniform CVP approach based on exponential spacing met all of the constraints throughout the SUGV's gliding flight in the provided cases, while the maximum values of the LF and Q for the non-uniform CVP technique in Table 3 could also be used to assess the impact of the increment on the number of nodes. To observe the superiority of the proposed non-uniform CVP, stopping values such as the stopping time t_s, gliding range R_g, and horizontal range R_h of the SUGV after hitting the ground could be compared with other referenced methods, which are listed in Table 4. It can be noted that the stopping time for the maximum step input was longer than the uniform and non-uniform CVP approaches because the pull-up condition avoided the free fall condition when releasing the SUGV from the carrier platform. Damping was slow due to unstable gliding flight, and because of this, the SUGV took longer to hit the ground. On the other hand, the uniform CVP approach suffered from the free-fall problem for nodes 10 and 15 after leaving the dispersion points, which caused unsteady gliding flight, whereas the uniform CVP for node 20 experienced a lower free fall condition, which caused an increase in the gliding range compared with nodes 10 and 15. It was also noticed that the suggested non-uniform CVP method required an average stopping time for the maximum gliding flight when compared with the maximum input and uniform

CVP approach because the non-uniform CVP approach successfully produced damped and steady gliding flight. Table 4 indicates that the non-uniform CVP approach outperformed the maximum step input and uniform CVP approach for R_g and R_h values higher than 121 km and 120 km, respectively.

Table 3. Maximum SUGV constraint values.

Constraints	Max δ_e	Uniform CVP			Non-Uniform CVP		
		$N = 10$	$N = 15$	$N = 20$	$N = 10$	$N = 15$	$N = 20$
α (deg)	4.6652	2.6480	2.6467	2.7040	2.6499	2.6500	2.6498
Q^L (deg s^{-1})	–5.2350	–1.9868	–1.9298	–1.9269	–1.0000	–0.9302	–0.9387
Q^U (deg s^{-1})	8.8224	1.0000	0.9761	1.0191	0.2654	0.3114	0.8970
LF	1.7466	1.2591	1.2199	1.2155	1.0069	1.0064	1.0063
δ_e (deg)	6.0000	5.8487	5.8464	5.9430	5.8522	5.8524	5.8521

Table 4. SUGV stopping values.

Stopping Values	Max δ_e	Uniform CVP			Non-Uniform CVP		
		$N = 10$	$N = 15$	$N = 20$	$N = 10$	$N = 15$	$N = 20$
t_s (s)	839.351	802.215	792.177	838.989	816.190	814.735	814.023
R_g (km)	118.556	120.141	119.901	120.282	121.250	121.259	121.278
R_h (km)	117.993	119.553	119.260	119.758	120.831	120.840	120.856

6. Conclusions

Instead of employing a time-scaling approach, the concept of considering the height as a stopping constraint was modified for the maximum stoppable time to achieve the maximum gliding range. To enhance the gliding range of an SUGV, a non-uniform CVP approach based on the notion of exponential spacing was presented to provide damped and steady gliding flight. The beauty of the proposed non-uniform CVP approach is that the exponential spacing via χ can be changed to suit the needs of the problem. The proposed CVP approach has no complicated preprocessing and is simple to implement. According to the simulation results, the proposed non-uniform CVP approach outperformed the uniform CVP approach in terms of optimal control throughout the gliding flight, ensuring damped and steady gliding flight and maximizing the gliding range. Increasing the node count in the CVP approach slowed down the rate of convergence and boosted the complexity of the optimizer. Compared with the maximum step input simulations, the proposed non-uniform CVP presented gliding flight with an increase of 2.722 km in the gliding range and 2.863 km in the horizontal range. The non-uniform CVP approach increased the gliding range by 1.377 km and the horizontal range by 1.098 km relative to the uniform CVP approach. Furthermore, the non-uniform CVP approach achieved a horizontal range 856 m higher than the horizontal range of 120 km given in the literature [6,34–36]. The efficacy and trustworthiness of the proposed non-uniform CVP approach were validated by simulations executed in the MATLAB and DS Simulia Isight environments. A six-DoF model of the SUGV can be utilized in the future to evaluate the viability of the proposed non-uniform CVP approach. To evaluate the proposed non-uniform CVP method, additional aero models will also be employed.

Author Contributions: Conceptualization, A.M. and A.I.B.; methodology, A.M., F.u.R. and A.I.B.; investigation, A.M.; writing—original draft preparation, A.M., F.u.R. and A.I.B.; writing—review and editing, A.M., F.u.R. and A.I.B.; visualization, A.M.; supervision, A.I.B. and F.u.R. All authors have read and agreed to the published version of the manuscript.

Funding: This research received no external funding.

Data Availability Statement: Not applicable.

Acknowledgments: The authors would like to acknowledge the Control and Signal Processing Research (CASPR) group of Capital University of Science and Technology in Islamabad, Pakistan. Special thanks to Imran Mir (Air University, Islamabad) and Bilal Ahmed Siddique (Woot Tech Aerospace, Pakistan) for sharing the data of gliding vehicles.

Conflicts of Interest: The authors declare no conflict of interest.

References

1. Hoffren, J.; Raivio, T. Optimal maneuvering after engine failure. In Proceedings of the Atmospheric Flight Mechanics Conference, Boston, MA, USA, 10–12 August 2000.
2. Rivas, D.; Franco, A.; Valenzuela, A. Optimization of unpowered descents for commercial aircraft. In Proceedings of the 11th AIAA Aviation Technology, Integration, and Operations (ATIO) Conference, Virginia Beach, VA, USA, 20–22 September 2011.
3. Wu, H.; Cho, N.C.; Bouadi, H.; Zhong, L.; Mora-Camino, F. Dynamic programming for trajectory optimization of engine-out transportation aircraft. In Proceedings of the 2012, 24th Chinese Control and Decision Conference (CCDC), Taiyuan, China, 23–25 May 2012.
4. Tola, C.; Beyazpinar, P.; Akin, D. Analysis of range extension process for outdated ballistic munitions ejected from an accelerator launcher concept. *J. Aviat.* **2021**, *5*, 90–100. [CrossRef]
5. Elsherbiny, A.; Bayoumy, A.; Elshabka, A.; Abdelrahman, M. Aerodynamic design optimization of range extension kit of a subsonic flying body. *J. Eng. Sci. Mil. Technol.* **2017**, *17*, 1–20. [CrossRef]
6. Mir, I.; Akhtar, S.; Eisa, S.A.; Maqsood, A. Guidance and control of standoff air-to-surface carrier vehicle. *Aeronaut. J.* **2019**, *123*, 283–309. [CrossRef]
7. Turco, K.T. Development of the Joint Stand Off Weapon (JSOW) Moving Target Capability: AGM-154 Block Three program. Master's Thesis, University of Tennessee, Knoxville, NT, USA, 2006.
8. Pullat, S.; Pushparaj, A. *Evolution of Smart Weapons*; National Institute of Advanced Studies: Bengaluru, India, 2019; pp. 1–28.
9. Sheu, D.; Chen, Y.-M.; Chang, Y.-J.; Chern, J.-S. Optimal glide for maximum range. In Proceedings of the 23rd Atmospheric Flight Mechanics Conference, Boston, MA, USA, 10–12 August 1998.
10. Sheu, D.; Chen, Y.-M.; Chern, J.-S. Optimal three-dimensional glide for maximum reachable domain. In Proceedings of the 24th Atmospheric Flight Mechanics Conference, Portland, OR, USA, 9–11 August 1999.
11. Chern, J.-S.; Ma, D.-M.; Vinh, N. Analytical solution for horizontal gliding flight. In Proceedings of the Atmospheric Flight Mechanics Conference, Hampton, VA, USA, 10–12 August 2000.
12. Kim, Y.; Kim, G.H.; Choi, J.-H. Optimal guidance for range maximization of guided projectile: The effects of autopilot delay and fin deployment timing on the flight range. In Proceedings of the 2019 International Conference on Unmanned Aircraft Systems (ICUAS), Atlanta, GA, USA, 11–14 June 2019.
13. Yu, W.; Chen, W. Guidance scheme for glide range maximization of a hypersonic vehicle. In Proceedings of the AIAA Guidance, Navigation, and Control Conference, Minneapolis, MN, USA, 13–16 August 2011.
14. Phillips, C.P. Guidance algorithm for range maximization and time-of-flight control of a guided projectile. *J. Guid. Control Dyn.* **2008**, *31*, 1447–1455. [CrossRef]
15. Zhang, D.-C.; Xia, Q.-L.; Wen, Q.-Q.; Zhou, G.-Q. An approximate optimal maximum range guidance scheme for subsonic unpowered gliding vehicles. *Int. Aerosp. Eng.* **2015**, *2015*, 1–8. [CrossRef]
16. Yuan, Y.B.; Zhang, K.; Xue, X.D. Optimization of glide trajectory of guided bombs using a Radau pseudo-spectral method. *Acta Armamentarii.* **2014**, *35*, 1179–1186.
17. Guo, K.; Xiong, F. Notice of retraction gliding trajectory optimization based on hp-adaptive pseudospectral method. In Proceedings of the 2013 International Conference on Quality, Reliability, Risk, Maintenance, and Safety Engineering (QR2MSE), Chengdu, China, 15–18 July 2013.
18. Qiu, W.; Jia, Q.; Meng, X.; Sun, Y. Maximum range trajectory optimization for a boost-glide vehicle using adaptive mesh refinement pseudospectral methods. *Proc. Inst. Mech. Eng. G J. Aerosp. Eng.* **2017**, *231*, 1171–1182. [CrossRef]
19. Gao, C.; Jiang, C.; Jing, W. Optimization of projectile state and trajectory of reentry body considering attainment of carrying aircraft. *J. Syst. Eng. Electron.* **2017**, *28*, 137–144. [CrossRef]
20. Xiao, L.; Lv, L.; Liu, P.; Liu, X.; Huang, G. A novel adaptive Gauss pseudospectral method for nonlinear optimal control of constrained hypersonic re-entry vehicle problem. *Int. J. Adapt. Control Signal Process.* **2018**, *32*, 1243–1258. [CrossRef]
21. An, K.; Guo, Z.-Y.; Xu, X.-P.; Huang, W. A framework of trajectory design and optimization for the hypersonic gliding vehicle. *Aerosp. Sci. Technol.* **2020**, *106*, 106110. [CrossRef]
22. Shapira, I.; Ben-Asher, J. Range maximization for emergency landing after engine cutoff. *J. Aircr.* **2005**, *42*, 1296–1306. [CrossRef]
23. Fang, X.; Wan, N.; Jafarnejadsani, H.; Sun, D.; Holzapfel, F.; Hovakimyan, N. Emergency landing trajectory optimization for fixed-wing UAV under engine failure. In Proceedings of the AIAA Scitech 2019 Forum, San Diego, CA, USA, 7–11 January 2019.
24. Harada, M.; Bollino, K. Optimal trajectory of a glider in ground effect and wind shear. In Proceedings of th AIAA Guidance, Navigation, and Control Conference and Exhibit, Monterey, CA, USA, 5–8 August 2005.
25. BenAsher, J.; Dekel, K.M. Pseudo-spectral-method based optimal glide in the event of engine Cut-off. In Proceedings of th AIAA Guidance, Navigation, and Control Conference, Portland, OR, USA, 8–11 August 2011.

26. Franco, A.; Rivas, D.; Valenzuela, A. Optimization of unpowered descents of commercial aircraft in altitude-dependent winds. *J. Aircr.* **2012**, *49*, 1460–1470. [CrossRef]
27. Nevrekar, A.; Striz, A.; Vedula, P. Maximum range glide of a supersonic aircraft in the presence of wind. In Proceedings of the 12th AIAA Aviation Technology, Integration, and Operations (ATIO) Conference and 14th AIAA/ISSMO Multidisciplinary Analysis and Optimization Conference, Indianapolis, IN, USA, 17–19 September 2012.
28. Segal, D.; Bar-Gill, A.; Shimkin, N. Max-range glides in engine cutoff emergencies under severe wind. *J. Guid. Control Dyn.* **2019**, *42*, 1822–1835. [CrossRef]
29. Bryson, J.; Vasile, J.D.; Celmins, I.; Fresconi, F. Approach for understanding range extension of gliding indirect fire munitions. In Proceedings of the 2018 Atmospheric Flight Mechanics Conference, Atlanta, GA, USA, 25–29 June 2018.
30. Vasile, J.D.; Bryson, J.; Gruenwald, B.C.; Fairfax, L.; Strohm, L.; Fresconi, F. A multi-disciplinary approach to design long range guided projectiles. In Proceedings of the AIAA Scitech 2020 Forum, Orlando, FL, USA, 6–10 January 2020.
31. Elsherbiny, A.M.; Aly, A.M.; Elshabka, A.; Abdelrahman, M. Modeling, simulation and hyprid optimization method as design tools for range extension kit of a subsonic flying body. In Proceedings of the 2018 AIAA Modeling and Simulation Technologies Conference, Kissimmee, FL, USA, 8–12 January 2018.
32. Vasile, J.D.; Bryson, J.; Fresconi, F. Aerodynamic design optimization of long range projectiles using missile DATCOM. In Proceedings of the AIAA Scitech 2020 Forum, Orlando, FL, USA, 6–10 January 2020.
33. Gaudet, B.; Drozd, K.; Furfaro, R. Adaptive approach phase guidance for a hypersonic glider via reinforcement meta learning. In Proceedings of the AIAA SCITECH 2022 Forum, San Diego, CA, USA, 3–7 January 2022.
34. Din, A.F.U.; Akhtar, S.; Maqsood, A.; Habib, M.; Mir, I. Modified model free dynamic programming: An augmented approach for unmanned aerial vehicle. *Appl. Intell.* **2022**,*52*, 1–21. [CrossRef]
35. Din, A.F.U.; Mir, I.; Gul, F.; Nasar, A.; Rustom, M.; Abualigah, L. Reinforced learning-based robust control design for unmanned aerial vehicle. *Arab. J. Sci. Eng.* **2022**, *47*, 1–16. [CrossRef]
36. Din, A.F.u.; Mir, I.; Gul, F.; Mir, S.; Saeed, N.; Althobaiti, T.; Abbas, S.M.; Abualigah, L. Deep Reinforcement Learning for integrated non-linear control of autonomous UAVs. *Processes* **2022**, *10*, 1307. [CrossRef]
37. Hull, D.G. Conversion of optimal control problems into parameter optimization problems. *J. Guid. Control Dyn.* **1997**, *20*, 57–60. [CrossRef]
38. Liu, H.; Teng, H.; Qiu, G.; Liu, P.; Yang, J. Gaussian discretization-based non-uniform control vector parameterization for terminal constrained hypersonic unmanned system trajectory optimization. In Proceedings of the 2020 Chinese Automation Congress (CAC), Shanghai, China, 6–8 November 2020.
39. Guo, J.; Li, B.; Ji, Y. A control parametrization based path planning method for the quad-rotor uavs. *J. Ind. Manag. Optim.* **2022**, *18*, 1079. [CrossRef]
40. Zhong, W.; Lin, Q.; Loxton, R.; Teo, K.L. Optimal train control via switched system dynamic optimization. *Optim. Methods Softw.* **2021**, *36*, 602–626. [CrossRef]
41. Liu, P.; Hu, Q.; Li, L.; Liu, M.; Chen, X.; Piao, C.; Liu, X. Fast control parameterization optimal control with improved Polak-Ribière-Polyak conjugate gradient implementation for industrial dynamic processes. *ISA Trans.* **2022**, *123*, 188–199. [CrossRef]
42. Hong, L.; Mo, Y.; Bao, D.; Gong, R. Chaos elite Harris hawk optimization algorithm to solve chemical dynamic optimization problems. *IEEE Access* **2022**, *10*, 65833–65853. [CrossRef]
43. Jin, L.; Yin, Y.; Loxton, R.; Lin, Q.; Liu, F.; Teo, K.L. Optimal control of nonlinear Markov jump systems by control parametrisation technique. *IET Control Theory Appl.* **2022**, *16*, 1–9. [CrossRef]
44. Liu, R.; Mo, Y.; Lu, Y.; Lyu, Y.; Zhang, Y.; Guo, H. Swarm-intelligence optimization method for dynamic optimization problem. *Mathematics* **2022**, *10*, 1803. [CrossRef]
45. Zhang, Y.; Mo, Y. Dynamic optimization of chemical processes based on modified sailfish optimizer combined with an equal division method. *Processes* **2021**, *9*, 1806. [CrossRef]
46. Xu, L.; Mo, Y.; Lu, Y.; Li, J. Improved seagull optimization algorithm combined with an unequal division method to solve dynamic optimization problems. *Processes* **2021**, *9*, 1037. [CrossRef]
47. Lyu, Y.; Mo, Y.; Lu, Y.; Liu, R. Enhanced beetle antennae algorithm for chemical dynamic optimization problems' non-fixed points discrete solution. *Processes* **2022**, *10*, 148. [CrossRef]
48. Chen, X.; Du, W.; Tianfield, H.; Qi, R.; He, W.; Qian, F. Dynamic optimization of industrial processes with nonuniform discretization-based control vector parameterization. *IEEE Trans. Autom. Sci. Eng.* **2014**, *11*, 1289–1299. [CrossRef]
49. Liu, P.; Liu, X.; Wang, P.; Li, G.; Xiao, L.; Yan, J.; Ren, Z. Control variable parameterisation with penalty approach for hypersonic vehicle reentry optimisation. *Int. J. Control* **2019**, *92*, 2015–2024. [CrossRef]
50. Teo, K.L.; Jepps, G.; Moore, E.J.; Hayes, S. A computational method for free time optimal control problems, with application to maximizing the range of an aircraft-like projectile. *J. Aust. Math. Soc. Series B Appl. Math.* **1987**, *28*, 393–413. [CrossRef]
51. Liu, H.; Liu, P.; Liu, X.; Huang, H. Adaptive control arc length-based time grid refinement control parameterisation method for unmanned hypersonic vehicle reentry trajectory optimisation. *Int. J. Control* **2022**, *95*, 1–11. [CrossRef]
52. Hui, X.; Guangbin, C.; Shengxiu, Z.; Xiaogang, Y.; Mingzhe, H. Hypersonic reentry trajectory optimization by using improved sparrow search algorithm and control parametrization method. *Adv. Space Res.* **2022**, *69*, 2512–2524. [CrossRef]
53. Lin, Q.; Loxton, R.; Teo, K.L.; Wu, Y.H. Optimal control problems with stopping constraints. *J. Glob. Optim.* **2015**, *63*, 835–861. [CrossRef]

54. Lin, Q.; Loxton, R.; Teo, K.L.; Wu, Y.H. Optimal control computation for nonlinear systems with state-dependent stopping criteria. *Automatica* **2012**, *48*, 2116–2129. [CrossRef]
55. Clancy, L.J. *Aerodynamics*; Longman: London, UK, 1986.